

Article

Optimal Capacity Configuration of Pumped-Storage Units Used to Retrofit Cascaded Hydropower Stations

Yang Li ^{1,*}, Feilong Hong ¹, Xiaohui Ge ², Xuesong Zhang ², Bo Zhao ² and Feng Wu ¹

¹ College of Energy and Electrical Engineering, Hohai University, Nanjing 211100, China; 221606030017@hhu.edu.cn (F.H.); wufeng@hhu.edu.cn (F.W.)

² State Grid Zhejiang Electric Power Company Research Institute, Hangzhou 310014, China; gexiaohui@dky.zj.sgcc.com.cn (X.G.); zhangxuesong@dky.zj.sgcc.com.cn (X.Z.); zhaobo@dky.zj.sgcc.com.cn (B.Z.)

* Correspondence: eeliyang@hhu.edu.cn

Abstract: As flexible resources, cascaded hydropower stations can regulate the fluctuations caused by wind and photovoltaic power. Constructing pumped-storage units between two upstream and downstream reservoirs is an effective method to further expand the capacity of flexible resources. This method transforms cascaded hydropower stations into a cascaded pumped-hydro-energy storage system. In this paper, a flexibility reformation planning model of cascaded hydropower stations retrofitted with pumped-storage units under a hybrid system composed of thermal, wind, and photovoltaic power is established with the aim of investigating the optimal capacity of pumped-storage units. First, a generative adversarial network and a density peak clustering algorithm are utilized to generate typical scenarios to deal with the seasonal fluctuation of renewable energy generation, natural water inflow, and loads. Then, a full-scenario optimization method is proposed to optimize the operation costs of multiple scenarios considering the variable-speed operation characteristics of pumped storage and to obtain a scheme with better comprehensive economy. Meanwhile, the proposed model is retransformed into a mixed-integer linear programming problem to simplify the solution. Case studies in Sichuan province are used to demonstrate the effectiveness of the proposed model.

Keywords: cascaded hydropower stations; renewable energy; optimal capacity configuration; pumped storage; variable-speed units; mixed-integer linear programming



Citation: Li, Y.; Hong, F.; Ge, X.; Zhang, X.; Zhao, B.; Wu, F. Optimal Capacity Configuration of Pumped-Storage Units Used to Retrofit Cascaded Hydropower Stations. *Energies* **2023**, *16*, 8049. <https://doi.org/10.3390/en16248049>

Academic Editor: Alban Kuriqi

Received: 6 November 2023

Revised: 30 November 2023

Accepted: 11 December 2023

Published: 13 December 2023



Copyright: © 2023 by the authors. Licensee MDPI, Basel, Switzerland. This article is an open access article distributed under the terms and conditions of the Creative Commons Attribution (CC BY) license (<https://creativecommons.org/licenses/by/4.0/>).

1. Introduction

With the continuous attention being paid to climate issues and the continuous consumption of fossil energy, many countries are gradually shifting their focus to renewable energy sources such as wind and photovoltaic (PV) power [1,2]. In particular, China has promised to achieve a carbon peak by 2030 and carbon neutrality by 2060, and wind and PV power generation are undoubtedly the preferred energy sources [3,4]. However, wind and PV power are greatly affected by environmental factors, making it difficult to accurately predict their power outputs. Therefore, the inherent uncertainties in wind and PV power generation challenge the safe and stable operation of power grids [5,6]. In this case, developing flexible resources has become effective and necessary [7,8].

Hydropower, with advantages such as controllable water reservoir volumes and mature technology, is an excellent regulating power source, and there exist temporal and spatial correlation characteristics between hydropower, wind power, and PV power generation which can promote the integration and development of wind and PV power [9,10]. Many scholars have conducted research on the complementary integration of hydropower, wind power, and PV power. Zhang et al. [11] captured the spatial and temporal correlations between wind and solar plants via an improved vine copula theory and demonstrated

the potential of a large-scale hydro–wind–solar hybrid system to meet export power transmission demands. Incorporating stochastic wind, solar, and small-hydro power, Biswas et al. [12] proposed a multi-objective economic-emission power dispatch problem formulation and solution and applied a decomposition-based multi-objective evolutionary algorithm and summation-based multi-objective differential evolution algorithm to comply with system constraints. Wei et al. [13] presented a stochastic optimization model considering the strong regulation capacity of cascade hydropower stations and the uncertainty of wind and PV power, which were solved with linearization methods and a proposed two-stage approach. From the above papers, it can be seen that hydropower plays a role in handling the problem of increasing renewable energy penetration, and it can be seen that a hybrid energy system (HES) is an effective method for promoting the consumption of renewable energy [14,15].

The above papers demonstrate the role of hydropower in mitigating the volatility of wind and PV power. In addition to hydropower, energy storage plays a role in dealing with the uncertainties of wind and PV power [16,17]. Sun et al. [18] proposed generalized demand-side resources by combining demand response with energy storage, presenting a configuration model to minimize operational costs in distribution networks. Li et al. [19] proposed an optimal scheduling method for minimizing operating costs in an isolated microgrid by addressing the uncertainty in spinning reserves from energy storage using chance-constrained programming.

Among the various type of energy storage, pumped-storage (PS) stations are increasingly gaining attention. As of the end of 2022, the global energy storage capacity reached 237.2 GW, with PS capacity accounting for 216.65 GW or 79.3%. In China, the energy storage capacity was 59.8 GW, with a PS capacity of 45.79 GW, accounting for 76.6% of the total. Huang et al. [20] exploited an approach to jointly scheduling generation and reserves for wind–solar–PS power systems and adopted a stochastic and finely adjustable robust optimization method considering discrete and continuous uncertainties. Jiang et al. [21] proposed a robust optimization approach to accommodate wind-output uncertainty and provide a robust unit commitment schedule for thermal generators; the total cost was reduced significantly by considering PS units. Kumar et al. [22] researched the optimal scheduling of a variable-speed pumped-storage (VSPS), solar and wind energy system and demonstrated that the net profit was increased by utilizing variable-speed technology.

In addition, scholars have conducted research into the optimal capacity configuration of PS stations. Nasir et al. [23] investigated the true potential of PS hydropower and its optimum operation, along with existing conventional hydropower, and optimized the capacity of PS hydropower. Diab et al. [24] presented an optimization method for sizing a hybrid system including PV and wind turbines with a hydroelectric PS system and investigated the implementation of different optimization techniques to achieve the optimal sizing of grid-connected hybrid renewable energy systems. Zhang et al. [25] introduced a rule-based method for determining PS regulation capacity, iteratively revising the PV curve to match the optimal PS regulation capacity, and explored the role of variable-speed and constant-frequency PS units in the joint power supply of cascaded hydropower and PV plants. Ren et al. [26] proposed a solution to grid instability and wastage in wind and PV systems by suggesting a combined PS/wind/PV/hydrogen production system, and this integration offered insights into optimizing energy storage capacities, contributing to stable and sustainable clean energy use.

According to the outline of the 14th Five-Year Plan proposed by the Chinese government, retrofitting cascaded hydropower stations (CHSs) with PS units—i.e., adding PS units between two upstream and downstream reservoirs—is an effective method to improve the flexibility of hydropower generation for renewable energy accommodation [27,28]. Hence, PS units can store and generate power by taking advantage of the reservoirs in hydropower plants (HPPs), and more and more research has shown the benefits of using existing reservoirs of HPPs as the reservoirs of PS units [29,30]. Some papers have already conducted research on PS retrofitting in cascaded hydropower generation. Wang et al. [31]

explored the complementary operation of the hybrid PS–wind–PV system at different time scales and evaluated the economic benefits and energy efficiency of the system. Ribeiro et al. [32] presented a model for a CHS which contained reversible turbines in several HPPs and considered the optimal problem under the framework of discrete-time optimal control. Toufani et al. [33] evaluated the benefits of CHSs retrofitted with reversible turbines, a system referred to as a pumped-hydro-energy storage (PHES) system, and the profits generated were analyzed. Hunt et al. [34] combined a large-scale pumped-storage site with a series of hydropower dams in cascade so the storage capacity could be obtained during the wet period. To enhance hydropower flexibility, Zhang et al. [35] evaluated the feasibility of adding a pumping station between two adjacent upstream and downstream reservoirs, and a large hydro–wind–solar clean energy base was considered. Similarly, by constructing pump stations between two adjacent upstream and downstream reservoirs, Ju et al. [36] transformed conventional CHSs into a pumped-hydro-energy storage system to integrate clean energy resources.

The above papers have primarily conducted research on the scheduling problem of CHSs retrofitted with PS, which is referred to as a cascaded pumped-hydro-energy storage system (CPHES), and there are few papers studying the PS capacity configuration problem of CPHES systems thus far. In this paper, the capacity optimization of PS units retrofitted in CHSs is investigated. A full-scenario optimization method is utilized to optimize the comprehensive operation costs of multiple scenarios of renewable energy generation, natural water inflow, and loads. The technology of VSPS is involved in the proposed model. In addition, the hydraulic constraints of PS operation are considered, and an efficient linearization method is proposed to decrease computational burdens.

The main contributions of this paper are as follows:

- A practical capacity configuration model of CHSs retrofitted with pumped-storage units is proposed, and linearization technologies are developed to address nonlinear constraints, improving computational efficiency.
- To deal with the seasonal fluctuation of renewable energy generation, natural water inflow, and loads, the scenario generation method based on generative adversarial network (GAN) and density peak clustering (DPC) algorithms with limited historical data are proposed, and a full-scenario optimization method is proposed to optimize the operation costs of multiple scenarios and obtain a scheme with better comprehensive economy.
- VSPS is considered in the CPHES system. Results demonstrate that PS units' retrofitting can reduce the curtailment of wind and PV power, relieve the peak-shaving pressure of thermal units, and reduce the frequent startup and shutdown of hydropower units. Furthermore, the advantage of VSPS units over fixed-speed pumped-storage (FSPS) units is verified.

The remaining sections are organized as follows: Section 2 establishes the system configuration of the hybrid energy system (HES) with CPHES; Section 3 presents the scenario generation algorithm and the capacity configuration optimization model; case studies are carried out in Section 4, and conclusions are provided in Section 5.

2. System Description

In a hybrid energy system, multiple resources such as hydropower, thermal power, wind power, and PV power are utilized. Thermal, wind, and PV power inject energy into the power grid. With the increasing penetration of wind and PV power generation, the possible curtailment of wind and PV power will occur due to their natural uncertainties and mismatch with load variation. In this case, excess curtailed power can be absorbed by PS units, stored in the reservoir, and then released to supply the peak load of the power grid.

A schematic of the hybrid energy system with CPHES is shown in Figure 1. It can be observed that HPP is integrated with PS units through a retrofitting process. Through constructing PS stations between cascade reservoirs, water can be pumped back to store energy, thereby absorbing excess electricity and reusing water. In this case, the existing reservoirs are well utilized. Therefore, the regulating ability of CHSs is enhanced with fewer

investment costs compared to rebuilding a new individual PS station. It should also be pointed out that the PS-retrofitted CHSs are not required to be located in the first and second reservoirs, as shown in Figure 1. The location of the PS should be determined depending on various factors like reservoir capacity and distance of upstream and downstream reservoirs.

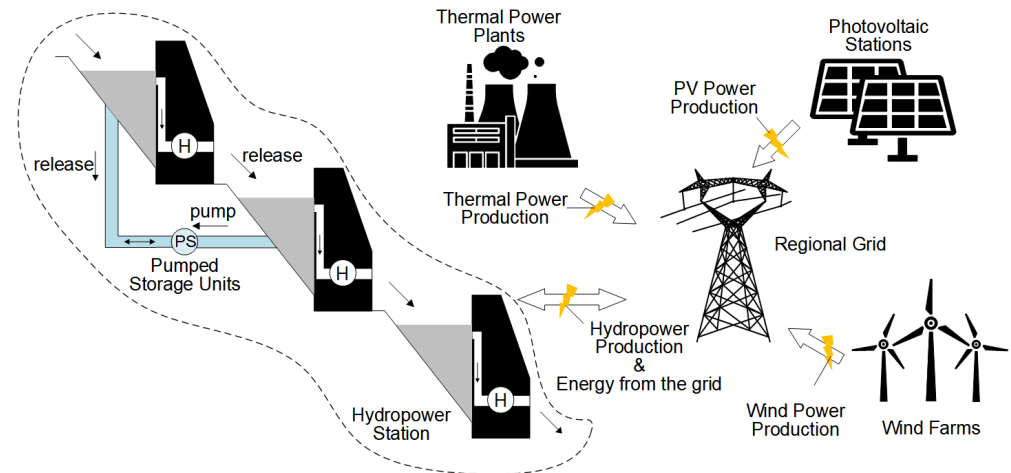


Figure 1. Schematic of the hybrid energy system with CPHEs.

The focus of this paper is to research the capacity of PS units and the role of PS units in the day-ahead scheduling of the power grid.

3. Modelling of the Proposed Hybrid System

3.1. Scenario Generation Method

The generation of scenarios regarding renewable energy generation, natural water inflow, and loads form the foundation for the configuration of PS units. This paper proposes a typical scenario generation method based on GAN and DPC algorithms, as illustrated in Figure 2.

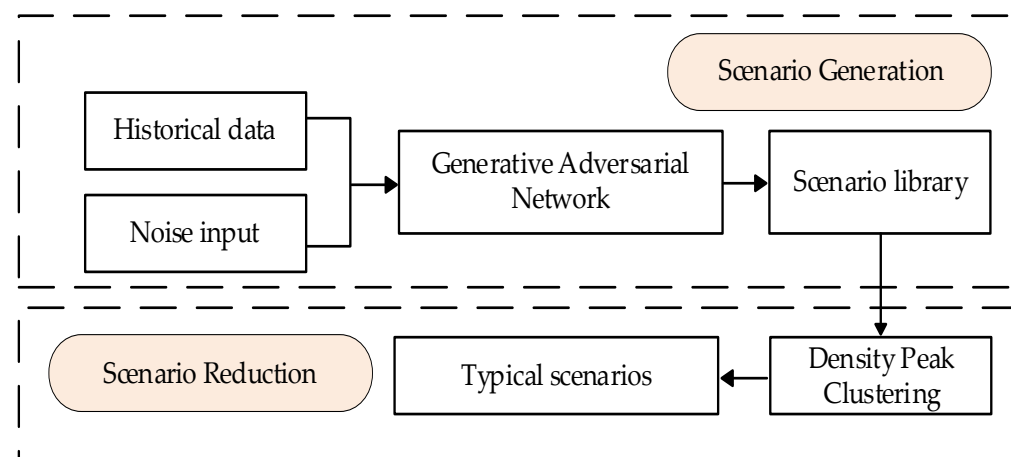


Figure 2. Procedure of scenario generation.

The specific steps are as follows:

- (1) Input historical data and alternately train GAN networks;
- (2) Generate a high number of data to establish a dataset of scenarios for wind and solar power output, natural water inflow, and loads;
- (3) Reduce scenarios based on the DPC algorithm to generate typical scenarios for the full-scenario operation optimization.

3.1.1. Generation of Scenario Database Based on GAN Algorithm

Renewable energy generation, natural water inflow, and loads have complicated correlations which are difficult to describe using traditional statistical methods. The advantage of GAN is that it can deeply explore the internal distribution patterns of input data, enabling the generated data to better describe the correlation characteristics of renewable energy generation, natural water inflow, and loads. The generation model is shown in Figure 3.

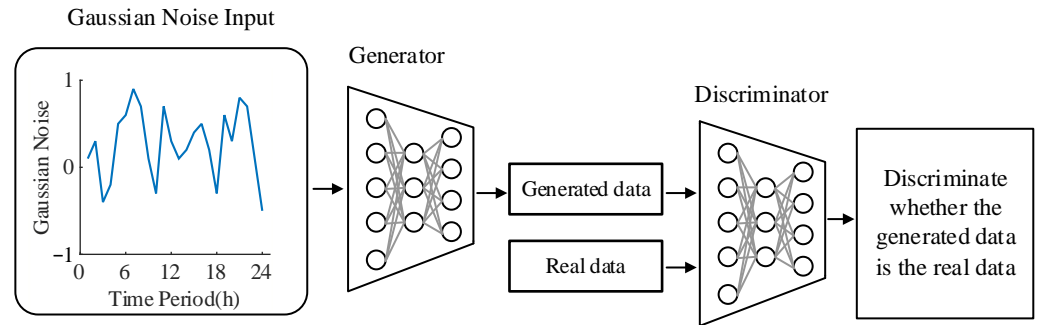


Figure 3. Scenario generation model based on GAN.

GAN is a data-driven machine learning model whose core lies in the game theory between generator G and discriminator D . The main task of the generator is to convert a set of unordered noise into a dataset as similar as possible to the input data, while the main task of the discriminator is to distinguish between the generated data and the real data as much as possible through learning from the input data. The loss function L_G of the generator and the loss function L_D of the discriminator are shown in (1) and (2), respectively:

$$L_G = -E_z[D(G(z, \theta_G), \theta_D)] \quad (1)$$

$$L_D = E_z[D(G(z, \theta_G), \theta_D)] - E_x[D(x, \theta_D)] \quad (2)$$

where z denotes the randomly generated noise; θ_G and θ_D denote the network parameters of generators and discriminators, respectively; $E_z[\cdot]$ denotes the expected value for generated data distribution; $G(\cdot, \theta_G)$ denotes the output value of the generator when the input value is noise z ; $D(\cdot, \theta_D)$ denotes the output value of the discriminator; x denotes real data for model training; and $E_x[\cdot]$ denotes the expected value of real data distribution.

The objective function $V(G, D)$ of the generator and discriminator is shown in (3):

$$\min_G \max_D V(G, D) = -E[D(G(z, \theta_G), \theta_D)] + E_x[D(x, \theta_D)] \quad (3)$$

3.1.2. Scenario Reduction Based on the DPC Algorithm

The DPC algorithm is a density-based clustering algorithm that offers a simpler computation process and does not involve an iterative procedure, in contrast to traditional algorithms like K-means. The DPC algorithm demonstrates better performance in computing non-spherical clusters and is less susceptible to noise interference. It is particularly suitable for data with high randomness, such as wind power and PV output. The core idea of this algorithm is to identify cluster centers with higher density compared to the surrounding points and that are a significant distance from other cluster centers.

The local density of any point i in the dataset is defined as:

$$\rho_i = \sum_j \chi(d_{ij} - d_c) \quad (4)$$

$$\chi(x) = \begin{cases} 1 & x < 0 \\ 0 & x \geq 0 \end{cases} \quad (5)$$

where $\chi(\cdot)$ denotes the defined logical judgment function; d_{ij} denotes the distance between point i and point j ; and d_c denotes the given truncation distance.

The minimum distance δ_i between point i and other higher density objects is defined as:

$$\delta_i = \min_{j:\rho_j > \rho_i} (d_{ij}) \tag{6}$$

If point i has the maximum local density, then δ_i is defined as:

$$\delta_i = \max_j (d_{ij}) \tag{7}$$

The specific steps are as follows:

First, calculating ρ_i of each data point;

Then, calculating δ_i of each data point;

Finally, drawing a decision graph with ρ_i as the x -axis and δ_i as the y -axis. The point in the upper right corner of the decision graph should be used as the center point of the cluster. This point should have high density and be far from other high-density points.

3.2. Objective Function

The cost of the HES includes the investment cost of installing PS units and the operation cost of each entity. The objective function aims to minimize the above costs; therefore, the objective function is as follows:

$$\min F = \min \{ F_B + F_C + F_H + F_{ps} + F_G \} \tag{8}$$

where F_B denotes the annualized investment cost of installing PS units; F_C , F_H , F_{ps} , and F_G , respectively, denote the annualized operation cost of wind and power, hydropower, PS, and thermal units.

3.2.1. Investment Cost

$$F_B = \frac{\eta_{ps}(1 + \eta_{ps})^{Y_{ps}}}{(1 + \eta_{ps})^{Y_{ps}} - 1} C_{ps} P^{ps} \tag{9}$$

where η_{ps} denotes the annual interest rate; Y_{ps} denotes the life of the PS unit; C_{ps} denotes the investment cost per unit capacity; and P^{ps} denotes the sum of the configured capacity of PS units.

3.2.2. The Penalty Cost of Wind and PV Power Curtailment

$$F_C = \sum_{m=1}^{12} D_m \sum_{t=1}^T [c_w (P_{m,t}^{W,f} - P_{m,t}^W) \Delta t + c_{pv} (P_{m,t}^{PV,f} - P_{m,t}^{PV}) \Delta t] \tag{10}$$

where D_m denotes the number of days in the month m ; T denotes the operating hours per typical day; c_w and c_{pv} are, respectively, the penalty cost coefficients of wind and PV curtailment; $P_{m,t}^{W,f}$ and $P_{m,t}^{PV,f}$ denote the day-ahead forecasted values of wind and PV power generation at time t of the typical day in month m , respectively; $P_{m,t}^W$ and $P_{m,t}^{PV}$ denote the day-ahead scheduling values of wind and PV power generation at time t of the typical day in month m , respectively; and Δt denotes the duration per time interval.

During the day-ahead dispatching process, it is desired that the predicted wind and PV power output are equal to the scheduled dispatching output, so there is a penalty cost associated with the difference between them.

3.2.3. The Operation Cost of Hydropower Units

$$F_H = \sum_{m=1}^{12} D_m \sum_{t=1}^T \sum_{i=1}^{N_H} \left[\sum_{j=1}^{J_i} u_{i,j,m,t}^H (1 - u_{i,j,m,t-1}^H) c_{i,j}^{H,u} + c_h Q_{i,m,t}^{qi} \Delta t \right] \quad (11)$$

where N_H is the number of CHSs; J_i is the number of hydropower units in HPP i ; $u_{i,j,m,t}^H$ is the binary variable that marks the operating status of hydropower unit j in HPP i at time t of the typical day in month m ; $c_{i,j}^{H,u}$ denotes the startup cost of hydropower unit j in HPP i ; c_h denotes the penalty cost coefficient of water spillage; and $Q_{i,m,t}^{qi}$ denotes the water discharge rate of HPP i at time t of the typical day in month m .

The operation cost of hydropower units generally consists of startup costs and water spillage cost. There will be no water spillage for HPPs during the non-flood seasons. Therefore, in the dispatching process, if water spillage occurs, a penalty cost is imposed upon it.

3.2.4. The Operation Cost of PS Units

$$F_{ps} = \sum_{m=1}^{12} D_m \sum_{t=1}^T \sum_{p=1}^{N_{ps}} [u_{p,m,t}^{psG} (1 - u_{p,m,t-1}^{psG}) c_p^{psG,u} + u_{p,m,t}^{psP} (1 - u_{p,m,t-1}^{psP}) c_p^{psP,u}] \quad (12)$$

where $u_{p,m,t}^{psG}$ and $u_{p,m,t}^{psP}$ are, respectively, the binary variables that mark the operating status of PS unit p in the generating and pumping condition at time t of the typical day in month m ; $c_p^{psG,u}$ and $c_p^{psP,u}$ denote the startup costs of PS unit p in the generating and pumping condition, respectively.

3.2.5. The Operation Cost of Thermal Units

Based on different regulatory capabilities and cost characteristics, the operation process of thermal units can be divided into three stages: regular peak regulation (RPR), deep peak regulation without oil (DPR), and deep peak regulation with oil (DPRO). As shown in Figure 4, the maximum power output and the minimum power output of the thermal unit during the RPR, DPR, and DPRO stages, respectively, are denoted by P_{max} , P_a , P_b , and P_c .

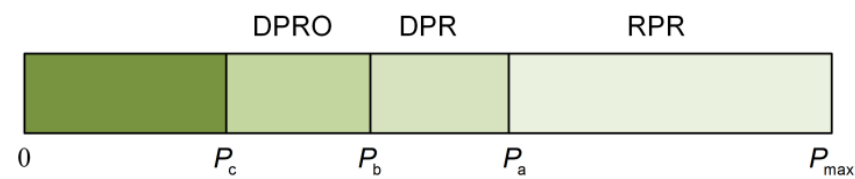


Figure 4. Schematic of peak shaving.

During the RPR period, the operation cost of thermal units only includes the coal cost, which is calculated by the coal consumption characteristic function $f_{coal}(\cdot)$ as follows:

$$f_{coal}(P) = (aP^2 + bP + c)S_{coal} \quad (13)$$

where a , b , and c , respectively, denote the coefficients of quadratic term, primary term, and constant term of the consumption characteristic function. Their values are related to the type of unit, boiler model, and coal quality; S_{coal} denotes the unit coal price in season, and P denotes the unit active power output.

During the DPR and DPRO stages, the thermal unit is prone to severe deformation and fracture, which shortens the lifespan of the unit. The calculation of rotor life is a very complex problem, and there is no recognized calculation formula in the existing research that can effectively solve it. This paper calculates the life loss of low-cycle fatigue according to the low-cycle fatigue characteristic of the rotor material.

The Manson coffin formula reflects the relationship between the total strain amplitude and the number of cycles of rotor cracking; its functional relationship is expressed as follows:

$$\Delta\varepsilon_t = \frac{\sigma_f}{E}(2N_t)^d + q_f(2N_t)^e \tag{14}$$

where σ_f denotes the fatigue strength coefficient of the material; q_f denotes the fatigue ductility coefficient of the material; d denotes the fatigue strength index of the material; e denotes the fatigue ductility index of the material; N_t denotes the cycle number of the rotor cracking at time t , which is related to unit output P ; $\Delta\varepsilon_t$ denotes the total strain amplitude of the rotor at time t ; and E denotes the elastic modulus.

The total strain amplitude $\Delta\varepsilon_t$ of the rotor can be obtained based on the stress and centrifugal tangential stress of the unit rotor, and substituting it into (14) can determine the number of cycles of rotor cracking N_t . Then, the unit loss cost $\omega_{\text{loss}}(P)$ combined with the unit purchase cost can be roughly calculated as follows:

$$\omega_{\text{loss}}(P) = \frac{1}{N_t} S_{\text{unit}} \tag{15}$$

where S_{unit} denotes the unit purchase cost.

During the DPRO stage, the boiler may experience unstable combustion, so the unit needs to be fed with oil to support combustion, ensuring safe operation of the unit. The oil input cost is expressed as follows:

$$\omega_{\text{oil}} = S_{\text{cost}} Z_{\text{oil}} \tag{16}$$

where S_{cost} denotes the unit fuel price in season, and Z_{oil} denotes the unit oil input.

Therefore, the operation costs of thermal power units in different peak-shaving stages feature different characteristics. The peak-shaving cost curve is shown in Figure 5, and the detailed peak-shaving cost of thermal power units can be expressed as a segmented function as follows:

$$C(P) = \begin{cases} f_{\text{coal}}(P) & P_a < P \leq P_{\text{max}} \\ f_{\text{coal}}(P) + \omega_{\text{loss}}(P) & P_b < P \leq P_a \\ f_{\text{coal}}(P) + \omega_{\text{loss}}(P) + \omega_{\text{oil}} & P_c < P \leq P_b \end{cases} \tag{17}$$

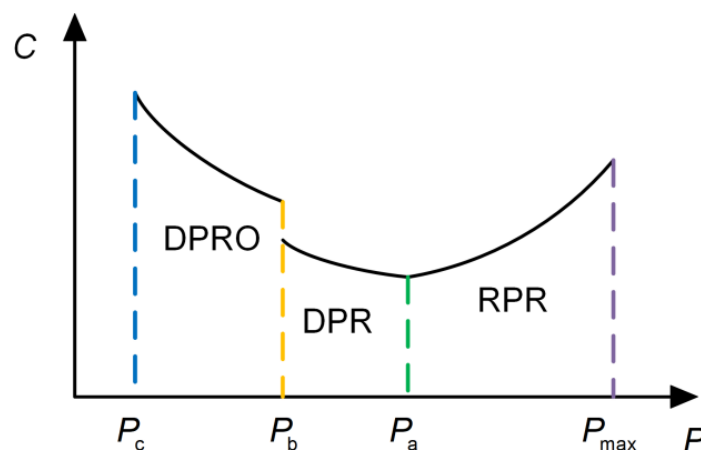


Figure 5. Schematic of peak-shaving cost.

The total cost of peak shaving for thermal power units is shown as follows:

$$F_{G1} = \sum_{m=1}^{12} D_m \sum_{t=1}^T \sum_{g=1}^{N_G} C(P_{g,m,t}^G) \tag{18}$$

where $P_{g,m,t}^G$ denotes the power output of thermal unit g at time t of the typical day in month m .

Then, the startup and shutdown costs of thermal units are defined as follows:

$$F_{G2} = \sum_{m=1}^{12} D_m \sum_{t=1}^T \sum_{g=1}^{N_G} [u_{g,m,t}^G (1 - u_{g,m,t-1}^G) C_g^{G,u} + u_{g,m,t-1}^G (1 - u_{g,m,t}^G) C_g^{G,d}] \quad (19)$$

where $u_{g,m,t}^G$ is the binary variable indicating the operating status of thermal unit g at time t of the typical day in month m , and $C_g^{G,u}$ and $C_g^{G,d}$ denote the startup and shutdown costs of thermal unit g , respectively.

In summary, the operation cost of thermal power units is shown as follows:

$$F_G = F_{G1} + F_{G2} \quad (20)$$

3.3. Constraints

3.3.1. Capacity Constraints of PS Units

$$P_{p,\min}^{\text{PS}} \leq P_p^{\text{PS}} \leq P_{p,\max}^{\text{PS}} \quad (21)$$

where $P_{p,\min}^{\text{PS}}$ and $P_{p,\max}^{\text{PS}}$ denote the minimum and maximum values of the configured capacity of PS unit p , respectively.

3.3.2. Balance Constraint of Power Output and Load

Matching the generation with the load is necessary in the power grid. The load balance constraints are shown in (22):

$$\sum_{i=1}^{N_H} \sum_{j=1}^{J_i} P_{i,j,m,t}^H + \sum_{p=1}^{N_{\text{ps}}} P_{p,m,t}^{\text{PSG}} + \sum_{g=1}^{N_G} P_{g,m,t}^G + P_{m,t}^W + P_{m,t}^{\text{PV}} = P_{m,t}^D + \sum_{p=1}^{N_{\text{ps}}} P_{p,m,t}^{\text{PSP}} \quad (22)$$

where $P_{p,m,t}^{\text{PSG}}$ and $P_{p,m,t}^{\text{PSP}}$, respectively, denote the power output of PS p in the generating and pumping condition at time t of the typical day in month m ; and $P_{m,t}^D$ denotes the day-ahead forecasted load at time t of the typical day in month m .

3.3.3. Constraints of Hydropower Units

Unit commitment constraints are shown in (23) and (24):

$$z_{i,j,m,t}^{\text{H,u}} - z_{i,j,m,t}^{\text{H,d}} = u_{i,j,m,t}^{\text{H}} - u_{i,j,m,t-1}^{\text{H}} \quad (23)$$

$$z_{i,j,m,t}^{\text{H,u}} + z_{i,j,m,t}^{\text{H,d}} \leq 1 \quad (24)$$

where $z_{i,j,m,t}^{\text{H,u}}$ and $z_{i,j,m,t}^{\text{H,d}}$ are binary variables indicating the startup and shutdown operation of hydropower unit j in HPP i at time t of the typical day in month m , respectively.

To reduce the computational complexity and computation time of the model, the average hydraulic head is considered in the generation model of hydropower units. Hydropower output constraints are as shown in (25) and (26):

$$P_{i,j,m,t}^H = \rho g \eta_{i,j}^H H_i q_{i,j,m,t}^H \quad (25)$$

$$u_{i,j,m,t}^{\text{H}} P_{i,j}^{\text{H,min}} \leq P_{i,j,m,t}^H \leq u_{i,j,m,t}^{\text{H}} P_{i,j}^{\text{H,max}} \quad (26)$$

where ρ denotes the water density; g denotes gravitational acceleration; $\eta_{i,j}^H$ denotes the power generation efficiency of hydropower unit j in HPP i ; H_i denotes the average hydraulic

head of HPP i ; and $P_{i,j}^{H,\min}$ and $P_{i,j}^{H,\max}$ denote the minimum and maximum power output of hydropower unit j in HPP i , respectively.

Taking into account the reliable operation and extended lifespan of hydropower units, as well as to ensure the stability and reliability of the power grid, it is necessary to consider the minimum startup and shutdown time of hydropower units as (27):

$$\begin{cases} (T_{i,j,\min}^{H,\text{on}} - T_{i,j,m,t-1}^{H,\text{on}})(u_{i,j,m,t}^H - u_{i,j,m,t-1}^H) \geq 0 \\ (T_{i,j,\min}^{H,\text{off}} - T_{i,j,m,t-1}^{H,\text{off}})(u_{i,j,m,t-1}^H - u_{i,j,m,t}^H) \geq 0 \end{cases} \quad (27)$$

where $T_{i,j,\min}^{H,\text{on}}$ and $T_{i,j,\min}^{H,\text{off}}$ denote the minimum running time and down time of hydropower unit j in HPP i , respectively, and $T_{i,j,m,t-1}^{H,\text{on}}$ and $T_{i,j,m,t-1}^{H,\text{off}}$ denote the continuous running time and down time of hydropower unit j in HPP i until time $t - 1$ of the typical day in month m , respectively.

3.3.4. Constraints of PS Units

PS units have two operating states, pumping and generating, and their commitment constraints are shown in (28)–(35):

$$u_{p,m,t}^{\text{psG}} + u_{p,m,t}^{\text{psP}} \leq 1 \quad (28)$$

$$z_{p,m,t}^{\text{psG,u}} - z_{p,m,t}^{\text{psG,d}} = u_{p,m,t}^{\text{psG}} - u_{p,m,t-1}^{\text{psG}} \quad (29)$$

$$z_{p,m,t}^{\text{psG,u}} + z_{p,m,t}^{\text{psG,d}} \leq 1 \quad (30)$$

$$z_{p,m,t}^{\text{psP,u}} - z_{p,m,t}^{\text{psP,d}} = u_{p,m,t}^{\text{psP}} - u_{p,m,t-1}^{\text{psP}} \quad (31)$$

$$z_{p,m,t}^{\text{psP,u}} + z_{p,m,t}^{\text{psP,d}} \leq 1 \quad (32)$$

$$\max \left\{ \sum_{t=1}^T z_{p,m,t}^{\text{psG,u}}, \sum_{t=1}^T z_{p,m,t}^{\text{psG,d}} \right\} \leq N_p^{\text{psG}} \quad (33)$$

$$\max \left\{ \sum_{t=1}^T z_{p,m,t}^{\text{psP,u}}, \sum_{t=1}^T z_{p,m,t}^{\text{psP,d}} \right\} \leq N_p^{\text{psP}} \quad (34)$$

$$\sum_{p' \neq p} u_{p',m,t}^{\text{psG}} \leq (N^{\text{ps}} - 1)(1 - u_{p,m,t}^{\text{psP}}) \quad (35)$$

where $z_{p,m,t}^{\text{psG,u}}$ and $z_{p,m,t}^{\text{psG,d}}$ are binary variables indicating the startup and shutdown action of PS unit p in generating conditions at time t of the typical day in month m , respectively; $z_{p,m,t}^{\text{psP,u}}$ and $z_{p,m,t}^{\text{psP,d}}$ are binary variables indicating the startup and shutdown action of PS unit p in the pumping condition at time t of the typical day in month m , respectively; N_p^{psG} and N_p^{psP} denotes the intraday maximum start–shut numbers of PS unit p in the generating and pumping condition, respectively.

A conventional FSPS plant comprises a pump turbine alongside upper and lower reservoirs. During periods of valley demands, the PS unit functions as a pump, consuming power to store water in the upper reservoir. Conversely, during periods of peak demands, it operates as a generator, supplying electricity by utilizing the stored water in the upper reservoir. Compared with the conventional FSPS unit, an outstanding characteristic of the VSPS unit lies in its ability to extensively adjust the speed of the pump turbine. This expands operational range to various input powers during the pumping mode while enhancing the overall efficiency of the system in the generating mode. Thus, regarding the modeling of FSPS and VSPS units, the FSPS unit is limited to a single fixed power point corresponding to a specific water head. As a result, the VSPS exhibits a broader power

tuning range. Considering dispatching requirements, these features present significant advantages for optimizing the operation of a hybrid power system.

Similar to the power output constraints in hydropower units, the average hydraulic head is also used for VSPS and FSPS units in order to simplify the model. The power output constraints of VSPSs are shown in (36)–(39):

$$P_{p,m,t}^{psG} = \rho g \eta_p^{psG,V} h_p q_{p,m,t}^{psG} \tag{36}$$

$$P_{p,m,t}^{psP} = \frac{\rho g h_p q_{p,m,t}^{psP}}{\eta_p^{psP,V}} \tag{37}$$

$$u_{p,m,t}^{psG} \alpha^{psG,V} P_p^{ps} \leq P_{p,m,t}^{psG} \leq u_{p,m,t}^{psG} P_p^{ps} \tag{38}$$

$$u_{p,m,t}^{psP} \alpha^{psP,V} P_p^{ps} \leq P_{p,m,t}^{psP} \leq u_{p,m,t}^{psP} P_p^{ps} \tag{39}$$

In comparison, power output constraints for FSPS units are shown in (40)–(43):

$$P_{p,m,t}^{psG} = \rho g \eta_p^{psG,F} h_p q_{p,m,t}^{psG} \tag{40}$$

$$P_{p,m,t}^{psP} = \frac{\rho g h_p q_{p,m,t}^{psP}}{\eta_p^{psP,F}} \tag{41}$$

$$P_{p,m,t}^{psP} = P_p^{ps} u_{p,m,t}^{psG} \tag{42}$$

$$u_{p,m,t}^{psG} \alpha^{psG,F} P_p^{ps} \leq P_{p,m,t}^{psG} \leq u_{p,m,t}^{psG} P_p^{ps} \tag{43}$$

where h_p denotes the average hydraulic head of PS units; $\eta_p^{psG,V}$ and $\eta_p^{psP,V}$, respectively, denote the power generation and pumping efficiency of VSPS unit p ; $\alpha^{psG,V}$ and $\alpha^{psP,V}$, respectively, denote the minimum power output coefficients of VSPS units in the generating and pumping condition; $\eta_p^{psG,F}$ and $\eta_p^{psP,F}$, respectively, denote the power generation and pumping efficiency of FSPS unit p ; and $\alpha^{psG,F}$ denotes the minimum power output coefficient of FSPS units in the generating condition.

3.3.5. Water Balance Constraints

In this paper, CHSs are retrofitted by PS. Water balance constraints with PS units' retrofitting are shown in (44)–(49):

$$V_{i,m,t} = V_{i,m,t-1} + (I_{i,m,t} + Q_{i-1,m,t}^{OUT} + Q_{m,t}^{ps} - \sum_{j=1}^{J_i} q_{i,j,m,t}^H - s_{i,m,t}) \Delta t \tag{44}$$

$$Q_{m,t}^{ps} = \begin{cases} 0 & , \text{ without PS} \\ \sum_{p=1}^{N_{ps}} (q_{p,m,t}^{psP} - q_{p,m,t}^{psG}) & , \text{ for PS's upper reservoir} \\ \sum_{p=1}^{N_{ps}} (q_{p,m,t}^{psG} - q_{p,m,t}^{psP}) & , \text{ for PS's lower reservoir} \end{cases} \tag{45}$$

$$Q_{i,m,t}^{OUT} = \sum_{j=1}^{J_i} q_{i,j,m,t} + s_{i,m,t} \tag{46}$$

$$0 \leq s_{i,m,t} \leq s_{i,max} \tag{47}$$

$$u_{i,j,m,t}^H q_{i,j}^{H,min} \leq q_{i,j,m,t}^H \leq u_{i,j,m,t}^H q_{i,j}^{H,max} \tag{48}$$

$$\begin{cases} u_{p,m,t}^{psG} q_p^{psG,min} \leq q_{p,m,t}^{psG} \leq u_{p,m,t}^{psG} q_p^{psG,max} \\ u_{p,m,t}^{psP} q_p^{psP,min} \leq q_{p,m,t}^{psP} \leq u_{p,m,t}^{psP} q_p^{psP,max} \end{cases} \quad (49)$$

where $V_{i,m,t}$ denotes the real-time reservoir storage capacity of HPP i at time t of the typical day in month m ; $I_{i,m,t}$ denotes the natural inflow rate of HPP i at time t of the typical day in month m ; $Q_{m,t}^{ps}$ denotes total water flow of PS at time t of the typical day in month m ; $q_{p,m,t}^{psG}$ and $q_{p,m,t}^{psP}$ denote the power flow and pumping flow rates of PS p at time t of the typical day in month m , respectively; $Q_{i,m,t}^{OUT}$ and $s_{i,m,t}$ denote the outflow and water spillage of HPP i at time t of the typical day in month m , respectively; $q_{i,j,m,t}^H$ denotes the hydro-turbine discharge water flow of hydropower unit j in HPP i at time t of the typical day in month m ; $s_{i,max}$ denotes the maximum water discharge water flow of HPP i ; $q_p^{psG,min}$ and $q_p^{psG,max}$, respectively, denote the minimum and maximum power flow of PS p ; and $q_p^{psP,min}$ and $q_p^{psP,max}$, respectively, denote the minimum and maximum pumping flow of PS p .

The water storage volume of reservoirs presents restrictions for achieving flood control: dead storage capacity, beneficial reservoir capacity, total reservoir capacity, etc. In addition, the initial and final values of the reservoir storage volume are usually fixed at the dispatching periods as (50):

$$\begin{cases} V_{i,min}^H \leq V_{i,m,t}^H \leq V_{i,max}^H \\ V_{i,0} = V_{i,T} \end{cases} \quad (50)$$

where $V_{i,min}^H$ and $V_{i,max}^H$ denote the minimum and maximum reservoir storage volumes of HPP i , respectively.

3.3.6. Constraints of Thermal Units

$$z_{g,m,t}^{G,u} - z_{g,m,t}^{G,d} = u_{g,m,t}^G - u_{g,m,t-1}^G \quad (51)$$

$$z_{g,m,t}^{G,u} + z_{g,m,t}^{G,d} \leq 1 \quad (52)$$

$$u_{g,m,t}^G P_{g,min}^G \leq P_{g,m,t}^G \leq u_{g,m,t}^G P_{g,max}^G \quad (53)$$

$$\begin{cases} \left(T_{g,min}^{G,on} - T_{g,m,t-1}^{G,on} \right) \left(u_{g,m,t}^G - u_{g,m,t-1}^G \right) \geq 0 \\ \left(T_{g,min}^{G,off} - T_{g,m,t-1}^{G,off} \right) \left(u_{g,m,t-1}^G - u_{g,m,t}^G \right) \geq 0 \end{cases} \quad (54)$$

where $z_{g,m,t}^{G,u}$ and $z_{g,m,t}^{G,d}$ are binary variables indicating the startup and shutdown operation of thermal unit g at time t of the typical day in month m , respectively; $u_{g,m,t}^G$ is the binary variable indicating the operating status of thermal unit g at time t of the typical day in month m ; $P_{g,min}^G$ and $P_{g,max}^G$ denote the minimum and maximum power output values of thermal unit g , respectively; $T_{g,min}^{G,on}$ and $T_{g,min}^{G,off}$ denote the minimum running time and down time of thermal unit g , respectively; and $T_{g,m,t-1}^{G,on}$ and $T_{g,m,t-1}^{G,off}$ denote the continuous running time and down time of thermal unit g until time $t - 1$ of the typical day in month m , respectively.

3.3.7. Constraints of Wind and PV Power Output

Under normal circumstances, the day-ahead scheduling values of wind and PV power generation should be less than or equal to the day-ahead forecasted values of wind and PV power generation, as shown in (55) and (56):

$$0 \leq P_{m,t}^W \leq P_{m,t}^{W,f} \quad (55)$$

$$0 \leq P_{m,t}^{PV} \leq P_{m,t}^{PV,f} \quad (56)$$

3.3.8. Reserve Constraints

Due to the inherent uncertainty of renewable energy sources, it is necessary to have reserve capacity in the grid to enhance the flexibility and robustness of the grid and ensure a reliable power supply. The reserve capacity for both hydropower units and thermal power units is considered in (57) and (58):

$$\begin{cases} \sum_{i=1}^{N_H} \sum_{j=1}^{J_i} (u_{i,j,m,t}^H P_{i,j}^{H,\max} - P_{i,j,m,t}^H) \geq \sigma P_{m,t}^D \\ \sum_{i=1}^{N_H} \sum_{j=1}^{J_i} (P_{i,j,m,t}^H - u_{i,j,m,t}^H P_{i,j}^{H,\min}) \geq \sigma P_{m,t}^D \end{cases} \quad (57)$$

$$\begin{cases} \sum_{g=1}^{N_G} (u_{g,m,t}^G P_{g,\max}^G - P_{g,m,t}^G) \geq \delta P_{m,t}^D \\ \sum_{g=1}^{N_G} (P_{g,m,t}^G - u_{g,m,t}^G P_{g,\min}^G) \geq \delta P_{m,t}^D \end{cases} \quad (58)$$

where σ and δ , respectively, denote the reserve coefficient of hydropower and thermal units.

3.4. Solving Algorithm

Since various nonlinear operational constraints are involved in the proposed model, the capacity optimization problem is a nonlinear optimization problem. Many methods, including Lagrangian relaxation (LR), dynamic programming (DP), and intelligent heuristics algorithms, have been applied to solve the hydropower scheduling-based problem. Many difficulties and challenges are encountered with the above methods [37]. For example, the problem of two or more reservoirs is enormously challenging for the DP-based method due to the curse of dimensionality. The nonlinear and nonconvex hydropower production functions make it very difficult for the LR framework to obtain the true dual function, meaning that the basis for algorithm convergence cannot be guaranteed as a result. Intelligent heuristic algorithms converge easily to a local optimal or even an infeasible solution [38,39].

In recent years, mixed-integer linear programming (MILP)-based approaches have been adopted by more and more researchers to solve the hydropower scheduling-based problem because of the availability of better-performing and more user-friendly commercial software with efficient solvers such as CPLEX 12.10.0 and Gurobi 11.0 [40–42]. Through incorporating the nonlinearities using piecewise linear approximation, the MILP approach was generally able to obtain reasonable results in an acceptable computational time [43].

3.4.1. The Linearization of the Coal Consumption Cost

Due to the quadratic term in the cost function of thermal power units, the relationship between coal consumption cost and thermal power output is nonlinear, so it is necessary to linearize it to simplify the model. The SOS-2 constraints can be used to handle the quadratic term here, and the detailed process of linearization can be seen in [44,45].

First, the thermal power output range can be divided into K intervals in equal steps:

$$\begin{cases} P_{g,\min}^G = P_g^{G,0} < \dots < P_g^{G,k} < \dots < P_g^{G,K+1} = P_{g,\max}^G \\ C_g^{\text{coal},k} = f_{\text{coal}}(P_g^{G,k}) \end{cases} \quad (59)$$

Then, by introducing continuous variables $w_{g,m,t}^k$ ($k = 1, 2, \dots, K + 1$), coal consumption cost and thermal power output can be denoted as follows, respectively:

$$\begin{cases} P_{g,m,t}^G = \sum_{k=1}^{K+1} w_{g,m,t}^k P_g^{G,k} \\ C_{g,m,t}^{\text{coal}} = \sum_{k=1}^{K+1} w_{g,m,t}^k f_{\text{coal}}(P_g^{G,k}) \end{cases} \quad (60)$$

To mark the interval in which $P_{g,m,t}^G$ is located, the binary variables $z_{g,m,t}^k$ ($k = 1, 2, \dots, K$) are introduced. When $z_{g,m,t}^k = 1$, $P_{g,m,t}^G$ is at the k -th interval; otherwise, when $z_{g,m,t}^k = 0$, $P_{g,m,t}^G$ is not at the k -th interval. The above variables satisfy the following constraints:

$$w_{g,m,t}^1 \leq z_{g,m,t}^1 \tag{61}$$

$$w_{g,m,t}^{K+1} \leq z_{g,m,t}^K \tag{62}$$

$$w_{g,m,t}^k \leq z_{g,m,t}^{k-1} + z_{g,m,t}^k \tag{63}$$

$$w_{g,m,t}^k \geq 0 \tag{64}$$

$$\sum_{k=1}^{K+1} w_{g,m,t}^k = 1 \tag{65}$$

$$\sum_{k=1}^K z_{g,m,t}^k = 1 \tag{66}$$

Through the above constraints, the nonlinear relationship between coal consumption cost and thermal power output has been transformed into a linear relationship, which simplifies the solving process of the model.

3.4.2. The Linearization of Power Constraints of PS Units

In the upper and lower power limit constraints of PS units, there are nonlinear terms formed by multiplying binary variables and linear variables ($u_{p,m,t}^{psG} P_p^{ps}$, $u_{p,m,t}^{psP} P_p^{ps}$), which need to linearize.

First, power consumption constraint is linearized. The continuous variable $w_{p,m,t}^{psG}$ is introduced to denote $u_{p,m,t}^{psG} P_p^{ps}$, i.e., $w_{p,m,t}^{psG} = u_{p,m,t}^{psG} P_p^{ps}$, the constraints on $w_{p,m,t}^{psG}$ are as follows:

$$\begin{cases} w_{p,m,t}^{psG} \leq P_p^{ps} \\ w_{p,m,t}^{psG} \geq P_p^{ps} - P_{p,max}^{ps} (1 - u_{p,m,t}^{psG}) \\ u_{p,m,t}^{psG} P_{p,min}^{ps} \leq w_{p,m,t}^{psG} \leq u_{p,m,t}^{psG} P_{p,max}^{ps} \end{cases} \tag{67}$$

Based on the above constraints, it can be seen that, when $u_{p,m,t}^{psG} = 0$, $w_{p,m,t}^{psG} = 0$; when $u_{p,m,t}^{psG} = 1$, $w_{p,m,t}^{psG} = P_p^{ps}$. The linearization can be completed by substituting $w_{p,m,t}^{psG}$ back to the original constraint:

$$\alpha_p^{psG} w_{p,m,t}^{psG} \leq P_{p,m,t}^{psG} \leq w_{p,m,t}^{psG} \tag{68}$$

Similarly, the above method can also be used to linearize the power consumption constraint of PS units:

$$\begin{cases} w_{p,m,t}^{psP} \leq P_p^{ps} \\ w_{p,m,t}^{psP} \geq P_p^{ps} - P_{p,max}^{ps} (1 - u_{p,m,t}^{psP}) \\ u_{p,m,t}^{psP} P_{p,min}^{ps} \leq w_{p,m,t}^{psP} \leq u_{p,m,t}^{psP} P_{p,max}^{ps} \end{cases} \tag{69}$$

The linearization can be completed by substituting $w_{p,m,t}^{psP}$ back into the original constraint:

$$\alpha_p^{psP} w_{p,m,t}^{psP} \leq P_{p,m,t}^{psP} \leq w_{p,m,t}^{psP} \tag{70}$$

To sum up, the model for optimal capacity configuration considering scheduling optimization is transformed into an MILP problem which can be solved by the Yalmip/Gurobi solver.

3.5. Optimization Model

The main information encompassed in the presented capacity optimization model in this paper is depicted in Figure 6. The input data include parameters of CHSs, parameters of thermal power units, and cost coefficients. The decision variables of the proposed model are divided into capacity configuration-related decision variables, which are the capacity of PS units, and operation-related variables such as the power outputs of thermal, hydropower, and PS units. As previously mentioned, the objective function comprises investment costs and operating costs, while the constraints include the operational constraints of each unit, electricity balance constraints, water balance constraints, and reserve constraints. Subsequently, the nonlinear parts mentioned were linearized and transformed into an MILP model for resolution.

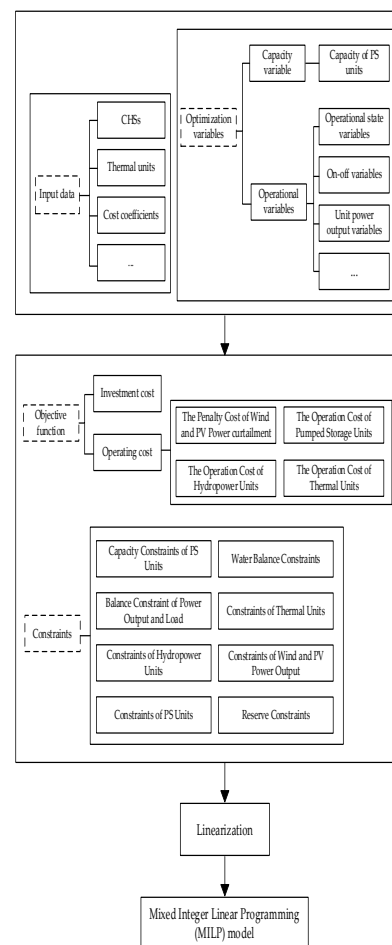


Figure 6. Schematic of system model.

4. Case Study

4.1. Case Parameters

In this paper, a hybrid energy system in the Sichuan province of China is applied to demonstrate the effectiveness and feasibility of this model. The system consists of hydropower units (448 MW of total installed capacity), thermal power units (440 MW of total installed capacity), wind farms (600 MW of total installed capacity), and PV stations (600 MW of total installed capacity).

The parameters of HPPs are shown in Table 1. The penalty cost coefficients of PV power and wind power curtailment are both set as USD 78.30/MWh, and the penalty cost coefficient of water spillage is USD 0.40/m³. The startup costs of hydropower and PS units are both set as USD 2.80/MW.

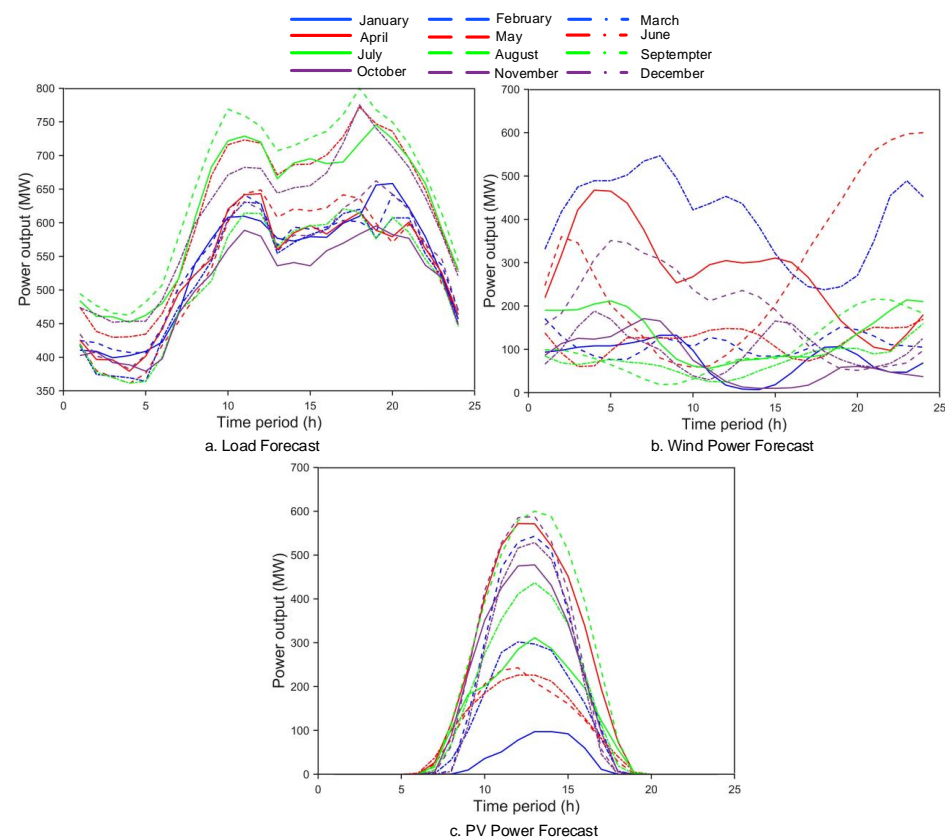
Table 1. Parameters of HPPs.

Symbol	HPP-1	HPP-2	HPP-3
Installed capacity (MW)	60×4	30×4	15×4
Minimum power output (MW)	14.7×4	6.4×4	5.6×4
Beneficial reservoir capacity (10^8 m^3)	9.35	0.15	0.16
Maximum hydro-turbine discharge rate (m^3/s)	51.53	18.63	0.16

In CHSs, the reservoir of HPP-1 is the main reservoir with the largest storage capacity in all cascade reservoirs. By controlling the water release of HPP-1, the operation of downstream reservoirs can be regulated. If PS units are constructed between the reservoirs of HPP-1 and HPP-2, controlling the entire downstream HPPs will be more convenient and effective. By constructing PS units using the existing reservoirs, the regulating capacity of reservoirs can be maximized to optimize the operation of the power system. In this case, a cascaded hydropower station is retrofitted with PS units between the reservoir of HPP-1 and the reservoir of HPP-2.

4.2. Analysis of Renewable Energy Generation, Natural Water Inflow, and Loads

Using combined GAN and DPC algorithms, 12 typical scenarios of renewable energy generation, power loads, and water inflow are generated as shown in Figures 7 and 8. In Figure 7a, it can be observed that the month with the highest load is August while the month with the lowest load is October, with a difference of approximately 200 MW. This indicates significant variations in load from month to month. Additionally, power load exhibits two peaks: a mid-day peak and an evening peak. The difference between the peak and valley loads is also significant, with the maximum value exceeding 300 MW. It is evident that the fluctuation in load poses challenges for capacity allocation of storage units and power system scheduling.

**Figure 7.** Forecasted load value, PV power output, and wind power output.

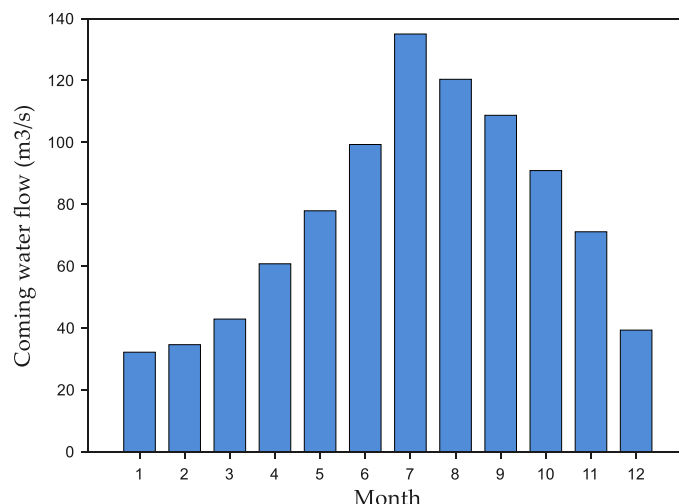


Figure 8. Natural inflow rate of HPP-1 monthly.

The forecasted wind power output curve for 12 typical days is shown in Figure 7b. Wind power output is characterized by significant volatility. The wind power output is larger at night and smaller during the daytime. However, during the late-night period, the load is at its lowest point of the day while wind power output tends to exceed the demand, resulting in curtailment of wind power. From the figure, it can also be seen that the month with the highest wind power output is March, but the load during this time is not the highest throughout the year.

Figure 7c shows the forecasted PV power output curve for 12 typical scenarios. As shown in the figure, PV power output is concentrated during the daytime. The maximum output occurs at noon, which provides a significant output for the peak load and exhibits a positive peak-shaving effect. Similar to wind power, it is evident that PV power generation also requires flexible resources to regulate its output. Otherwise, it may lead to unstable grid operation and curtailment of PV power.

Figure 8 shows the natural inflow rate of HPP-1; it can be seen from the figure that in the months during the summer and autumn seasons, natural flow rates are relatively high, and HPPs can generate a large amount of electricity, which is precisely matched with the high regional grid load at this stage. In other months, natural inflow rates are relatively small, resulting in a decrease in the power output of HPPs.

Based on the analysis above, it is evident that regions with large-scale wind power and PV power generation require flexible resources. This paper transforms CHSs into a CPHES, which can enhance the system's regulation capacity. The specific advantages of this approach will be analyzed below.

4.3. Optimal Capacity Configuration and Result Analysis of Scheduling

After being solved by the solver, the capacity configuration result of the PS units is 58.55×3 (MW), and the sum of annual investment and operation cost is USD 34,088,289.11, while the annual operation cost of the system without PS is USD 43,524,357.96. In contrast, operational costs with PS units have decreased by 21.68%. It can be seen that although the investment cost is relatively high, after the regulation of PS units, the system operation cost decreases, greatly improving the economy of the system's operation.

To illustrate the effectiveness of the model described in this paper, the following section will analyze the specific advantages of a CPHES. The model includes 12 typical days to obtain better comprehensive economy. Here, three typical days are selected for analysis. The optimal scheduling results of HESs with and without retrofitted PS units are shown in Figure 9.

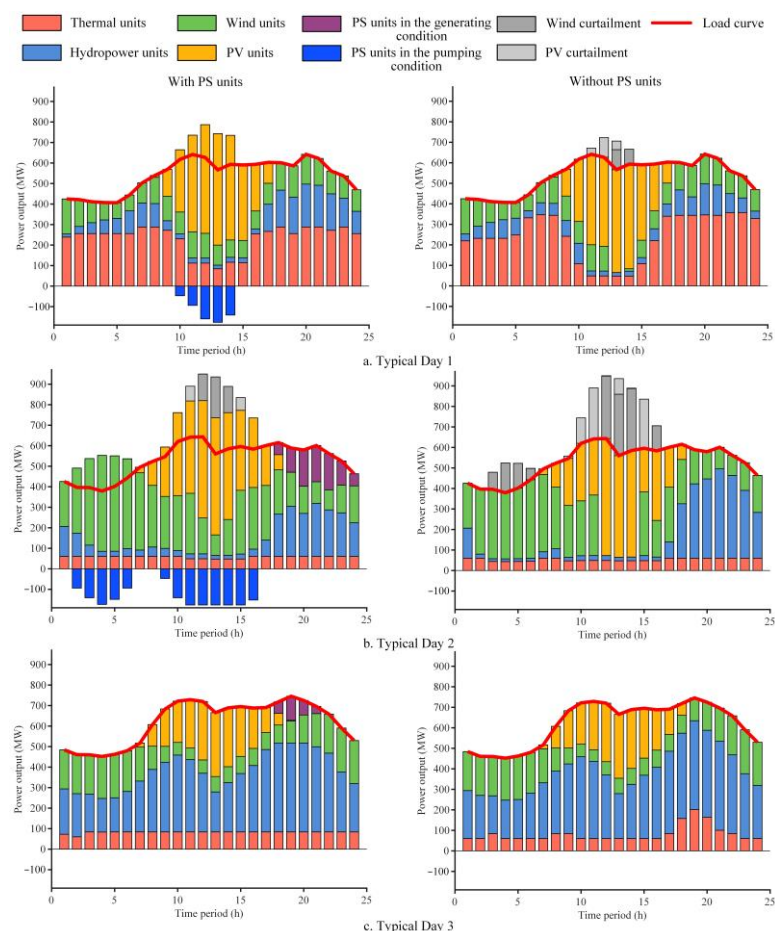


Figure 9. Optimal scheduling results on typical days.

From Figure 9a,b, it can be seen that through the regulation of PS units, the curtailment rate of wind and PV power is greatly reduced. When the system is not retrofitted with PS units, the curtailments of wind and PV power are 4852 MWh and 1663 MWh, respectively. By contrast, the hybrid system retrofitted with PS units reduces the curtailment of wind and PV power to 630 MWh and 387 MWh, respectively. The total curtailment of wind and PV power has decreased by 84.39%.

In addition, PS units can reduce the peak-shaving pressure of thermal power units. Due to the requirement of the spinning reserve, there is at least one thermal unit in operation. When the output of renewable energy is high, thermal units need to reduce output or even enter the state of deep peak shaving. However, if retrofitted with PS units, cascaded hydropower stations can operate in the pumping condition. Then, thermal units can avoid or reduce the duration of being in the state of deep peak shaving, which can, accordingly, reduce the cost of system operation and lengthen the service life of thermal units. As shown in Figure 9a, in the case without retrofitted PS units, there is one thermal unit in the deep peak-shaving state during the 11:00–14:00 period. However, for retrofitted PS units, there are no thermal units operating in the deep peak-shaving state in this typical day. As shown in Figure 9b, in the case without PS units, a thermal unit is in the deep peak-shaving state during the periods of 03:00–06:00 and 09:00–16:00, while in the system with PS units, the thermal unit operates in the deep peak-shaving state during the 11:00 to 15:00 period. Overall, in the case without retrofitted PS units, the deep peak-shaving cost of thermal units is USD 6,094,914.86. In contrast, the deep peak-shaving cost is reduced to USD 4,638,992.60 when retrofitted with PS units, demonstrating a 23.89% reduction.

PS units increase the generating capacity of hydropower stations, thus reducing the power output of thermal units during peak-load periods. From Figure 9c, it can be seen that

when not retrofitted with PS units, the hydropower unit has reached its maximum output in the evening peak-load period. Then, the power load is satisfied by increasing the power output of thermal units, which, in turn, increases the operation cost of the thermal units.

Finally, retrofitting with PS units can also reduce the frequent startup and shutdown of hydropower units. In the case of systems without PS units, when wind and PV power output is high, hydropower units reduce wind and PV power curtailment by reducing their own power output and shutting down their units, which inevitably increases the startup and shutdown cost of hydropower units. In contrast, when systems are retrofitted with PS units, when wind and PV power output is high, PS units operate in pumping conditions, ensuring that hydropower units remain in operation, which not only reduces the frequent startup and shutdown cost of hydropower units but also reduces wind and PV power curtailment. Although the startup and shutdown costs of PS units is USD 39,428.68, the startup and shutdown cost of hydropower units is decreased from USD 319,791.73 to USD 191,271.02, and the total cost is decreased by 27.86%.

4.4. Effects of VSPS Units

VSPS units can quickly respond to grid demands, adjust the output power, and achieve the most efficient energy conversion. The following analysis will focus on the effects of VSPS units in CPHEs and demonstrate the advantages of the VSPS over FSPS units.

By involving FSPS units in the model, the capacity configuration results of FSPS units can be obtained after solving the model.

From Table 2, it can be seen that when retrofitted with FSPS units, the annualized total cost will reach USD 39,053,653.35, which is greater than the cost of the case retrofitted with VSPS units. Additionally, due to an increase in the configured capacity, the investment cost also increases. Compared to VSPS units, the operation costs of both hydropower and thermal power units in hybrid systems retrofitted with FSPS units increase. However, the operation costs of PS units and curtailed energy decrease. This is because FSPS units have less frequent startups and shutdowns and larger configured capacity, resulting in a significant increase in total cost due to the reduction in these factors. Therefore, considering the factors mentioned above, VSPS units have an advantage over FSPS units.

Table 2. Costs comparison.

Costs	Variable-Speed PS Units	Fixed-Speed PS Units
Annualized total cost (USD)	34,088,289.11	39,053,653.35
Configured capacity (MW)	58.55 × 3	61.25 × 3
Investment cost (USD)	6,025,020.01	6,303,425.05
The operation cost of hydropower units (USD)	191,271.02	274,826.26
The operation cost of thermal units (USD)	25,442,736.61	25,573,435.92
The operation cost of PS units (USD)	39,428.68	37,750.86
Energy curtailment (MWh)	1017	954

5. Conclusions

In this paper, an optimal capacity configuration model of PS units retrofitted between two upstream and downstream reservoirs is established. A full-scenario scheduling framework is proposed for the hybrid energy system consisting of CPHEs systems, taking seasonal fluctuation of renewable energy generation, loads, and water inflow into consideration. Linearization technologies are employed to reduce computational burdens. Case studies from the Sichuan province of China are explored, and the effects of PS retrofitting are demonstrated by comparing the annualized total cost and scheduling of hybrid systems with and without retrofitted PS units. The specific conclusions are as follows:

- (1) The fluctuation of renewable energy generation is considered in the proposed capacity configuration optimization problem. Combined GAN and DPC algorithms are utilized to generate typical scenarios to balance the computational burdens and accuracy.
- (2) Retrofitting a cascaded hydropower station with PS units can increase the regulation capacity of hydropower stations. In turn, the curtailment of wind and PV power

can be reduced, the peak-shaving pressure of thermal units can be relieved, and the frequency of startups and shutdowns of hydropower units can also be reduced.

- (3) VSPPS units possess greater advantages than FSPS units in terms of retrofitting CHSs into a CPHESS system to improve the feasibility of CHSs.

Future work will study the influence of multiple uncertainties on the optimal capacity and scheduling of CPHESSs.

Author Contributions: Conceptualization, Y.L. and F.H.; methodology, Y.L.; software, F.H. and X.G.; validation, Y.L. and F.H.; formal analysis, F.W.; investigation, Y.L.; resources, Y.L.; data curation, X.Z.; writing—original draft preparation, F.H. and X.G.; writing—review and editing, F.W. and B.Z.; visualization, Y.L.; supervision, Y.L.; project administration, Y.L. All authors have read and agreed to the published version of the manuscript.

Funding: This research was funded by a technology project “Research on integration and coordinated generation and storage control technology of distributed pumped storage power plants” by State Grid Zhejiang Electric Power Co., Ltd., grant number 5211DS22000P.

Data Availability Statement: Data are contained within the article.

Conflicts of Interest: Authors Xiaohui Ge, Xuesong Zhang, Bo Zhao were employed by the company State Grid Zhejiang Electric Power Company Research Institute. The remaining authors declare that the research was conducted in the absence of any commercial or financial relationships that could be construed as a potential conflict of interest. The authors declare that this study received funding from State Grid Corporation of China. The funder was not involved in the study design, collection, analysis, interpretation of data, the writing of this article or the decision to submit it for publication. The authors declare no conflict of interest.

References

- Liu, C.H.; Chau, K.T.; Zhang, X.D. An Efficient Wind-Photovoltaic Hybrid Generation System Using Doubly Excited Permanent-Magnet Brushless Machine. *IEEE Trans. Ind. Electron.* **2010**, *57*, 831–839.
- Rahardja, F.A.; Chen, S.C.; Rahardja, U. Review of Behavioral Psychology in Transition to Solar Photovoltaics for Low-Income Individuals. *Sustainability* **2022**, *14*, 1537. [[CrossRef](#)]
- Li, M.Q.; Virguez, E.; Shan, R.; Tian, J.L.; Gao, S.; Patiño-Echeverri, D. High-resolution data shows China’s wind and solar energy resources are enough to support a 2050 decarbonized electricity system. *Appl. Energy* **2022**, *306*, 117996. [[CrossRef](#)]
- Qiu, S.; Lei, T.; Wu, J.T.; Bi, S.S. Energy demand and supply planning of China through 2060. *Energy* **2021**, *234*, 121193. [[CrossRef](#)]
- Shezan, S.A.; Kamwa, I.; Ishraque, M.F.; Muyeen, S.M.; Hasan, K.N.; Saidur, R.; Rizvi, S.M.; Shafiullah, M.; Al-Sulaiman, F.A. Evaluation of Different Optimization Techniques and Control Strategies of Hybrid Microgrid: A Review. *Energies* **2023**, *16*, 1792. [[CrossRef](#)]
- Cao, Z.A.; Wang, J.K.; Zhao, Q.; Han, Y.H.; Li, Y.C. Decarbonization Scheduling Strategy Optimization for Electricity-Gas System Considering Electric Vehicles and Refined Operation Model of Power-to-Gas. *IEEE Access* **2021**, *9*, 5716–5733. [[CrossRef](#)]
- Ding, T.; Wu, Z.Y.; Lv, J.J.; Bie, Z.H.; Zhang, X.J. Robust Co-Optimization to Energy and Ancillary Service Joint Dispatch Considering Wind Power Uncertainties in Real-Time Electricity Markets. *IEEE Trans. Sustain. Energy* **2016**, *7*, 1547–1557. [[CrossRef](#)]
- Lu, R.Z.; Ding, T.; Qin, B.Y.; Ma, J.; Fang, X.; Dong, Z.Y. Multi-Stage Stochastic Programming to Joint Economic Dispatch for Energy and Reserve with Uncertain Renewable Energy. *IEEE Trans. Sustain. Energy* **2020**, *11*, 1140–1151. [[CrossRef](#)]
- Wang, Z.N.; Wen, X.; Tan, Q.F.; Fang, G.H.; Lei, X.H.; Wang, H.; Yan, J.Y. Potential assessment of large-scale hydro-photovoltaic-wind hybrid systems on a global scale. *Renew. Sust. Energy Rev.* **2021**, *146*, 111154. [[CrossRef](#)]
- Danso, D.K.; François, B.; Hingray, B.; Diedhiou, A. Assessing hydropower flexibility for integrating solar and wind energy in West Africa using dynamic programming and sensitivity analysis. Illustration with the Akosombo reservoir, Ghana. *J. Clean Prod.* **2021**, *287*, 125559. [[CrossRef](#)]
- Zhang, H.X.; Lu, Z.X.; Hu, W.; Wang, Y.T.; Dong, L.; Zhang, J.T. Coordinated optimal operation of hydro-wind-solar integrated systems. *Appl. Energy* **2019**, *242*, 883–896. [[CrossRef](#)]
- Biswas, P.P.; Suganthan, P.N.; Qu, B.Y.; Amaratunga, G.A.J. Multiobjective economic-environmental power dispatch with stochastic wind-solar-small hydro power. *Energy* **2018**, *150*, 1039–1057. [[CrossRef](#)]
- Wei, H.; Zhang, H.X.; Yu, D.; Wang, Y.T.; Ling, D.; Ming, X. Short-term optimal operation of hydro-wind-solar hybrid system with improved generative adversarial networks. *Appl. Energy* **2019**, *250*, 389–403. [[CrossRef](#)]
- Zhu, Z.A.; Wang, X.; Jiang, C.W.; Wang, L.L.; Gong, K. Multi-objective optimal operation of pumped-hydro-solar hybrid system considering effective load carrying capability using improved NBI method. *Int. J. Electr. Power Energy Syst.* **2021**, *129*, 106802. [[CrossRef](#)]

15. Lu, L.; Yuan, W.L.; Su, C.G.; Wang, P.L.; Cheng, C.T.; Yan, D.H.; Wu, Z.N. Optimization model for the short-term joint operation of a grid-connected wind-photovoltaic-hydro hybrid energy system with cascade hydropower plants. *Energy Conv. Manag.* **2021**, *236*, 114055. [[CrossRef](#)]
16. Kong, Y.G.; Kong, Z.G.; Liu, Z.Q.; Wei, C.M.; Zhang, J.F.; An, G.C. Pumped storage power stations in China: The past, the present, and the future. *Renew. Sust. Energy Rev.* **2017**, *71*, 720–731. [[CrossRef](#)]
17. Caralis, G.; Papantonis, D.; Zervos, A. The role of pumped storage systems towards the large scale wind integration in the Greek power supply system. *Renew. Sust. Energy Rev.* **2012**, *16*, 2558–2565. [[CrossRef](#)]
18. Sun, W.Q.; Gong, Y.; Luo, J. Energy Storage Configuration of Distribution Networks Considering Uncertainties of Generalized Demand-Side Resources and Renewable Energies. *Sustainability* **2023**, *15*, 1097. [[CrossRef](#)]
19. Li, Y.; Yang, Z.; Li, G.Q.; Zhao, D.B.; Tian, W. Optimal Scheduling of an Isolated Microgrid with Battery Storage Considering Load and Renewable Generation Uncertainties. *IEEE Trans. Ind. Electron.* **2019**, *66*, 1565–1575. [[CrossRef](#)]
20. Huang, H.Y.; Zhou, M.; Zhang, L.J.; Li, G.Y.; Sun, Y.K. Joint generation and reserve scheduling of wind-solar-pumped storage power systems under multiple uncertainties. *Int. Trans. Electr. Energy Syst.* **2019**, *29*, e12003. [[CrossRef](#)]
21. Jiang, R.W.; Wang, J.H.; Guan, Y.P. Robust Unit Commitment with Wind Power and Pumped Storage Hydro. *IEEE Trans. Power Syst.* **2012**, *27*, 800–810. [[CrossRef](#)]
22. Kumar, R.; Kumar, A. Optimal scheduling of variable speed pumped storage, solar and wind energy system. *Energy Sources Part A-Recovery Util. Environ. Eff.* **2021**, 1–16. [[CrossRef](#)]
23. Nasir, J.; Javed, A.; Ali, M.; Ullah, K.; Kazmi, S.A.A. Capacity optimization of pumped storage hydropower and its impact on an integrated conventional hydropower plant operation. *Appl. Energy* **2022**, *323*, 119561. [[CrossRef](#)]
24. Diab, A.A.Z.; Sultan, H.M.; Kuznetsov, O.N. Optimal sizing of hybrid solar/wind/hydroelectric pumped storage energy system in Egypt based on different meta-heuristic techniques. *Environ. Sci. Pollut. Res.* **2020**, *27*, 32318–32340. [[CrossRef](#)] [[PubMed](#)]
25. Zhang, S.; Xiang, Y.; Liu, J.Y.; Liu, J.C.; Yang, J.X.; Zhao, X.; Jawad, S.; Wang, J. A Regulating Capacity Determination Method for Pumped Storage Hydropower to Restrain PV Generation Fluctuations. *CSEE J. Power Energy Syst.* **2022**, *8*, 304–316.
26. Ren, Y.; Jin, K.Y.; Gong, C.L.; Hu, J.Y.; Liu, D.; Jing, X.; Zhang, K. Modelling and capacity allocation optimization of a combined pumped storage/wind/photovoltaic/hydrogen production system based on the consumption of surplus wind and photovoltaics and reduction of hydrogen production cost. *Energy Conv. Manag.* **2023**, *296*, 117662. [[CrossRef](#)]
27. Sospiro, P.; Nibbi, L.; Liscio, M.C.; De Lucia, M. Cost-Benefit Analysis of Pumped Hydroelectricity Storage Investment in China. *Energies* **2021**, *14*, 8322. [[CrossRef](#)]
28. Sun, Q.J.; Zhou, J.Y.; Lan, Z.; Ma, X.Y. The Economic Influence of Energy Storage Construction in the Context of New Power Systems. *Sustainability* **2023**, *15*, 3070. [[CrossRef](#)]
29. Kucukali, S. Finding the most suitable existing hydropower reservoirs for the development of pumped-storage schemes: An integrated approach. *Renew. Sust. Energy Rev.* **2014**, *37*, 502–508. [[CrossRef](#)]
30. Kocaman, A.S.; Modi, V. Value of pumped hydro storage in a hybrid energy generation and allocation system. *Appl. Energy* **2017**, *205*, 1202–1215. [[CrossRef](#)]
31. Wang, Z.N.; Fang, G.H.; Wen, X.; Tan, Q.F.; Zhang, P.; Liu, Z.H. Coordinated operation of conventional hydropower plants as hybrid pumped storage hydropower with wind and photovoltaic plants. *Energy Conv. Manag.* **2023**, *277*, 116654. [[CrossRef](#)]
32. Ribeiro, A.F.; Guedes, M.C.M.; Smirnov, G.V.; Vilela, S. On the optimal control of a cascade of hydro-electric power stations. *Electr. Power Syst. Res.* **2012**, *88*, 121–129. [[CrossRef](#)]
33. Toufani, P.; Nadar, E.; Kocaman, A.S. Operational benefit of transforming cascade hydropower stations into pumped hydro energy storage systems. *J. Energy Storage* **2022**, *51*, 104444. [[CrossRef](#)]
34. Hunt, J.D.; Freitas, M.A.V.; Pereira, A.O. Enhanced-Pumped-Storage: Combining pumped-storage in a yearly storage cycle with dams in cascade in Brazil. *Energy* **2014**, *78*, 513–523. [[CrossRef](#)]
35. Zhang, J.T.; Cheng, C.T.; Yu, S.; Shen, J.J.; Wu, X.Y.; Su, H.Y. Preliminary feasibility analysis for remaking the function of cascade hydropower stations to enhance hydropower flexibility: A case study in China. *Energy* **2022**, *260*, 125163. [[CrossRef](#)]
36. Ju, C.; Ding, T.; Jia, W.H.; Mu, C.G.; Zhang, H.J.; Sun, Y.G. Two-stage robust unit commitment with the cascade hydropower stations retrofitted with pump stations. *Appl. Energy* **2023**, *334*, 120675. [[CrossRef](#)]
37. Cheng, C.T.; Su, C.G.; Wang, P.L.; Shen, J.J.; Lu, J.Y.; Wu, X.Y. An MILP-based model for short-term peak shaving operation of pumped-storage hydropower plants serving multiple power grids. *Energy* **2018**, *163*, 722–733. [[CrossRef](#)]
38. Guisández, I.; Pérez-Díaz, J.I. Mixed integer linear programming formulations for the hydro production function in a unit-based short-term scheduling problem. *Int. J. Electr. Power Energy Syst.* **2021**, *128*, 106747. [[CrossRef](#)]
39. Tong, B.; Zhai, Q.Z.; Guan, X.H. An MILP Based Formulation for Short-Term Hydro Generation Scheduling with Analysis of the Linearization Effects on Solution Feasibility. *IEEE Trans. Power Syst.* **2013**, *28*, 3588–3599. [[CrossRef](#)]
40. Cheng, C.T.; Wang, J.Y.; Wu, X.Y. Hydro Unit Commitment with a Head-Sensitive Reservoir and Multiple Vibration Zones Using MILP. *IEEE Trans. Power Syst.* **2016**, *31*, 4842–4852. [[CrossRef](#)]
41. Li, X.; Li, T.J.; Wei, J.H.; Wang, G.Q.; Yeh, W.W.G. Hydro Unit Commitment via Mixed Integer Linear Programming: A Case Study of the Three Gorges Project, China. *IEEE Trans. Power Syst.* **2014**, *29*, 1232–1241. [[CrossRef](#)]
42. Connolly, D.; Lund, H.; Finn, P.; Mathiesen, B.V.; Leahy, M. Practical operation strategies for pumped hydroelectric energy storage (PHES) utilising electricity price arbitrage. *Energy Policy* **2011**, *39*, 4189–4196. [[CrossRef](#)]

43. Finardi, E.C.; Takigawa, F.Y.K.; Brito, B.H. Assessing solution quality and computational performance in the hydro unit commitment problem considering different mathematical programming approaches. *Electr. Power Syst. Res.* **2016**, *136*, 212–222. [[CrossRef](#)]
44. Vielma, J.P.; Nemhauser, G.L. Modeling disjunctive constraints with a logarithmic number of binary variables and constraints. *Math. Program.* **2011**, *128*, 49–72. [[CrossRef](#)]
45. Ferreira, R.S.; Borges, C.L.T.; Pereira, M.V.F. A Flexible Mixed-Integer Linear Programming Approach to the AC Optimal Power Flow in Distribution Systems. *IEEE Trans. Power Syst.* **2014**, *29*, 2447–2459. [[CrossRef](#)]

Disclaimer/Publisher’s Note: The statements, opinions and data contained in all publications are solely those of the individual author(s) and contributor(s) and not of MDPI and/or the editor(s). MDPI and/or the editor(s) disclaim responsibility for any injury to people or property resulting from any ideas, methods, instructions or products referred to in the content.